Adaptive Fault Interruption Coordination in DC Microgrids Based on Current Rise Rate

Moein Ghadrdan[a], Daniel Dsa[b], Satish Naik Banavath[b], and Giovanni De Carne[a]
[a]*institute for technical physics, karlsruhe institute of technology,* Karlsruhe, Germany
[b]*department of electrical, electronics, and communication engineering, indian institute of technology dharwad,* Dharwad, India
{moein.ghadrdan, giovanni.carne}@kit.edu, {daniel.dsa, satish}@iitdh.ac.in.

***Abstract*—DC microgrids are increasingly recognized as a promising solution for enabling an efficient and reliable energy transition. However, their widespread deployment remains constrained by the inherent complexity of DC microgrid protection. The short length and low inductance of DC distribution lines, combined with large DC-link capacitors, result in extremely steep short-circuit current transients with rates of rise reaching several hundreds of amperes per microsecond, leaving a very limited time window for fault detection, interruption, and selective operation. This paper proposes a novel protection coordination strategy for radial DC microgrids that employs the rate of rise of fault current as the primary coordination parameter. In contrast to most existing approaches, which rely mainly on the absolute magnitude of fault current and face inherent limitations in DC systems, the proposed method investigates the feasibility of using the fault current slope as the key coordination metric and establishes systematic criteria for determining appropriate threshold settings for circuit breakers at different locations within the microgrid. The proposed strategy is validated through comprehensive simulation studies under various grid configurations and load conditions, and the results demonstrate effective coordination of multiple circuit breakers using the proposed threshold-setting framework, ensuring selectivity, and fast fault isolation.**

Keywords— DC circuit breaker, DC-link capacitor, fault coordination, rate-of-rise, protection

I. Introduction

Protection in DC power systems has long been considered challenging due to the absence of natural current zero-crossings, the sustained presence of electrical arcs during fault interruption, and the substantially higher rate of rise of fault currents compared with AC systems [1]. Recent progress in DC circuit breaker (CB) technologies, particularly the development of solid-state [2] and hybrid topologies [3], has alleviated the first two challenges to a large extent by enabling rapid and arc-free fault interruption. However, the extremely fast escalation of fault currents remains a critical unresolved issue, significantly complicating the design of reliable fault detection schemes and the coordinated operation of CBs in DC networks.

The rapid rise of fault current in DC systems primarily originates from the combination of low line inductance, due to short cable lengths, and the presence of large DC-link capacitors. While short-circuit faults in AC systems typically evolve over several tens to hundreds of milliseconds, a solid pole-to-pole fault in a DC microgrid can exhibit current rise rates on the order of hundreds of amperes per microsecond. Such transient behavior dramatically reduces the available time for fault detection, decision-making, and protection coordination, rendering conventional protection approaches ineffective. Overall, the high rate of rise of DC fault current results in two fundamental challenges associated with fault detection and protection coordination in DC systems.

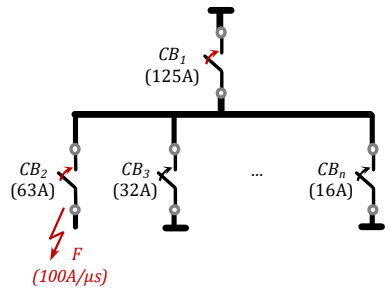

Fig. 1. Coordination mismatch between upstream and downstream CBs.

1. The first challenge is associated with the accurate measurement of the fault-current magnitude. Current sensors are typically limited in bandwidth, resulting in attenuation of high-frequency components in the measured signal. In addition, although the series inductance of such sensors is generally only a few nanohenries, under fault conditions characterized by extremely high rates of current rise, this small inductance gives rise to a significant measurement error. For example, when a 1-mΩ shunt resistor is used for fault-current measurement, the parasitic inductance of this shunt resistor (e.g., approximately 2 nH) introduces an additional voltage drop. For a fault current exhibiting a di/dt of 500 A/µs, the voltage across this parasitic inductance reaches 1 V, which corresponds to an apparent error of approximately 1000 A in the inferred current.
2. The second major challenge is related to the loss of selectivity in interruption coordination strategies that rely solely on the fault-current magnitude. As illustrated in Fig. 1, such approaches are prone to misoperation under conditions of extremely high fault-current rise rates. In the shown example, the downstream circuit breaker is configured with a current threshold of 63 A, while the upstream breaker is set to 125 A. For fault-current rise rates on the order of 100 A/µs, which are fully realistic in most DC applications, the fault current exceeds the upstream breaker threshold during the inherent delay of approximately 2 µs between fault detection and interruption by the downstream breaker, a typical value for solid-state circuit breakers. Consequently, both breakers are triggered, resulting in unnecessary upstream interruption and the disconnection of a large portion of the DC network [4].

Current interruption coordination strategies in DC grids are largely derived from the i^2t-based approaches originally developed for AC systems [5]. Traditional fault-interruption devices, such as electromagnetic CBs and fuses, rely on mechanical or sacrificial elements that operate based on the energy released during a fault, making energy-based coordination methods appropriate for such systems. In contrast, most modern DC protection technologies, including solid-state and hybrid CBs, utilize electronic sensing mechanisms that detect

979-8-3315-7502-1/26/$31.00 ©2026 IEEE

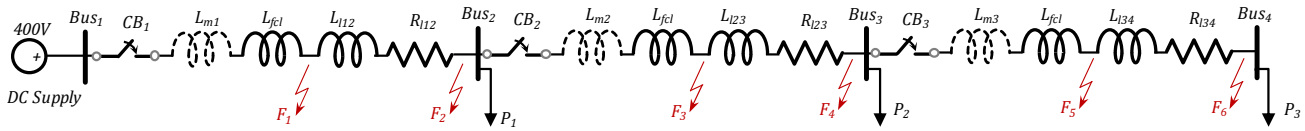

Fig. 2. Single-line diagram of the evaluated sample DC microgrid.

threshold crossings rather than accumulated energy. This fundamental difference suggests that new coordination strategies could be developed to enable ultra-fast and more effective interruption in DC networks.

To improve the robustness of fault detection in DC systems, several previous studies have investigated the use of the rate of rise of fault current (di/dt) as the primary fault indicator, rather than relying on the absolute value of the fault current [6]-[7]. By employing di/dt-based detection, the adverse impact of parasitic inductances associated with current sensors can be significantly reduced, as the fault indicator is derived directly from the transient behavior of the current rather than from its instantaneous magnitude. In addition, the rate of rise of current exhibits inherently higher sensitivity to fault inception compared to fault current magnitude, since the maximum di/dt in the fault loop typically occurs immediately following fault initiation. As a result, fault detection can be achieved at an earlier stage, before the fault current reaches high absolute levels, enabling faster reactions.

The primary objective of this study is to investigate the feasibility of extending the use of the fault-current rate of rise beyond fault detection to serve as the main coordination signal governing the operation of CBs in DC microgrids. Achieving this objective requires the development of a systematic coordination framework in which di/dt thresholds are defined such that CBs located electrically closer to the fault are guaranteed to operate faster than upstream devices. Since the maximum di/dt typically occurs immediately after fault occurrence, this approach is inherently well suited to address the aforementioned challenge of protection coordination, particularly under fault conditions characterized by extremely steep current transients. By exploiting the spatial variation of current rise rates along the feeder, selective operation can be achieved even in scenarios where conventional magnitude-based coordination becomes ineffective.

Despite these advantages, the use of di/dt as the primary coordination parameter also introduces potential limitations that must be carefully considered. In conventional magnitude-based protection schemes, backup protection is inherently provided, as a failure of the downstream CB results in a continued increase of the fault current until the threshold of the upstream CB is exceeded, allowing fault isolation at higher hierarchical levels. In contrast, di/dt-based coordination may compromise this backup functionality, since the rate of rise of current of some of breakers is highest at the fault moment and may never exceed upstream thresholds if the downstream CB fails to operate. Nevertheless, this limitation can be mitigated through appropriate threshold selection that explicitly accounts for both the faster and higher di/dt observed at locations closer to the fault. By incorporating these dependencies into the coordination design, selective operation can still be achieved while preserving a degree of backup protection within the di/dt-based framework.

The second complication concerns the accurate acquisition of the fault-current rate of rise. When di/dt is obtained through numerical differentiation of measured fault-current magnitude, required high sampling rates make the calculated signal highly sensitive to measurement noise. Moreover, the use of repeated measurements and filtering to suppress noise inevitably increases detection latency, which is particularly detrimental in DC systems with extremely fast fault transients. These limitations represent a key reason why di/dt-based approaches have often been avoided in practical fault detection schemes. In this work, however, the voltage across dedicated measurement inductors is utilized as a direct physical representation of di/dt, thereby avoiding numerical differentiation and significantly improving robustness. This approach introduces an additional degree of freedom in the protection design, as coordination can be systematically achieved through appropriate sizing of the measurement inductors, enabling selective operation without compromising detection speed.

The remainder of this paper is organized as follows. Section II presents the proposed protection coordination framework and derives the reaction thresholds for representative radial DC microgrid configurations with different load types and locations. Section III provides comprehensive simulation results for the considered configurations and validates the effectiveness of the proposed threshold-definition methodology. Finally, Section IV concludes the paper and summarizes the main findings.

II. Fault Current Derivative-Based Coordination

This section aims to develop an analytical framework for determining di/dt-based fault detection thresholds for different DC circuit breakers in a DC microgrid. In AC systems, fault detection thresholds are typically derived from extensive load-flow analyses under multiple contingency scenarios. Although similar simulation-based approaches can be applied to DC networks, this section focuses on a simplified analytical formulation to determine threshold values of the fault current di/dt. The proposed method enables systematic threshold selection while simultaneously facilitating the sizing of the measurement inductors required for coordinated DC fault detection.

To support this objective, a simplified representative DC microgrid, adopted from [5], is considered (Fig. 2). Three fundamental operating scenarios are analyzed on this test system through circuit-level analytical modeling and time-domain simulation. The system is configured as a radial network, where a CB is installed at the beginning of each section. Each CB integrates a Fault Current Limiter (FCL) (L_{fcl}), and the distribution lines are modelled using a series combination of resistance and inductance ($L_{li,j}$, $R_{li,j}$). The parameters of the DC network, transmission lines, and the FCL are

TABLE I. SPECIFICATIONS OF THE SAMPLE MICROGRID

Parameter	Value
Line di/dt @ 400V	2000A/µs/m
Line Specific Resistance	0.15mΩ/m
FCL di/dt @ 400V	100A/µs
Length l_{12}, l_{23}, l_{34}	100, 120, 150 meters

summarized in Table I. Assuming the nominal DC bus voltage, inductances are translated into their equivalent fault di/dt.

In many DC network studies, loads are commonly modeled as constant active power elements, without explicitly defining their physical characteristics. However, the input capacitors of end-use converters can significantly influence the fault current, and therefore may affect di/dt-based coordination performance. To examine this effect, three scenarios are evaluated for the sample radial DC network of Fig. 2. In the first scenario, a single purely resistive load is connected at the end of the line, serving as the base case for comparison. In the second scenario, resistive loads are connected to all buses. Finally, the third scenario considers a more realistic load representation, where a resistive load in parallel with its input capacitor is connected to each bus.

A. Single Loop Fault Evolution

This scenario considers a single resistive load (P_3) at the end of the feeder, with P_1 and P_2 set to zero. Therefore, wherever a fault occurs, all the upstream CBs experience similar di/dt, and the current in the remaining breakers drops to zero. The threshold set based on this scenario represents the minimum value, as the absence of DC-link capacitors limits the rate of rise of fault current. In the first stage of analysis, measurement inductors (L_{mi}) in Fig. 2 are excluded from the calculations. When a fault occurs at the beginning of line l_{12} (F_1), the di/dt experienced by CB_1 corresponds to the maximum derivative permitted by the fault current limiter.

$$F_1 \rightarrow (di/dt)_{@CB_1} = (di/dt)_{fcl} \quad (1)$$

Next, if a fault occurs at the end of line l_{12} (denoted as F_2), the di/dt experienced by CB_1 can be determined as follows:

$$F_2 \rightarrow (di/dt)_{@CB_1} = \left(\frac{1}{(di/dt)_{fcl}} + \frac{1}{(di/dt)_{l12}}\right)^{-1} \quad (2)$$

Considering identical fault current limiters, the rate of rise of fault current can also be illustrated through examples for faults at locations F_3 and F_5, calculated as follows:

$$F_3 \rightarrow (di/dt)_{@CB_1,CB_2} = \left(\frac{2}{(di/dt)_{fcl}} + \frac{1}{(di/dt)_{l12}}\right)^{-1} \quad (3)$$

$$F_5 \rightarrow (di/dt)_{@CB_1,CB_2,CB_3} = \left(\frac{3}{(di/dt)_{fcl}} + \frac{1}{(di/dt)_{l12}} + \frac{1}{(di/dt)_{l23}}\right)^{-1} \quad (4)$$

As shown in (3) and (4), in a microgrid with a single load at the end of the feeder, all upstream circuit breakers experience identical fault current di/dt, representing the worst-case scenario for di/dt-based coordination. To ensure robustness of the proposed protection strategy under diverse operating conditions, small measurement inductors are integrated into each circuit breaker (L_{mi}). The voltage across these inductors provides an accurate representation of the di/dt detected by each CB. Also, by employing inductors with different inductance values, prioritized protection zones can be effectively coordinated as the CBs at the end of the line are equipped with larger measurement inductances capable of reaching higher thresholds, while upstream CBs utilize smaller inductances. Measurement inductors with graded inductance values guarantee that only the inductor voltage of the circuit breaker nearest to the fault exceeds the detection threshold.

TABLE II. COORDINATION STRATEGY PERFORMANCE EVALUATION (SINGLE LOOP SCENARIO)

	Voltage across L_{mi} (V)			Does CB react?		
Location	$V(L_{m1})$	$V(L_{m2})$	$V(L_{m3})$	CB_1	CB_2	CB_3
F_1	10	< 0	< 0	✓	✗	✗
F_2	1.666	< 0	< 0	✓	✗	✗
F_3	1.428	3.142	< 0	✗	✓	✗
F_4	0.769	1.692	< 0	✗	✓	✗
F_5	0.714	1.571	2.642	✗	✗	✓
F_6	0.465	1.023	1.720	✗	✗	✓

When selecting measurement inductors, it is first necessary to ensure that their inductances remain sufficiently small compared to the corresponding line inductances. Moreover, by choosing proportionally scaled measurement inductors, a single unified detection threshold can be employed across the entire system, thereby simplifying protection design. To establish a unified threshold across all CBs, the measurement inductance integrated with each CB must be sized according to the distance between the furthest point within the section it protects and the main source.

As an illustrative example, the test network shown in Fig. 2 is evaluated using the parameters listed in Table I. Based on the corresponding line lengths, the measurement inductances L_{m1}, L_{m2}, and L_{m3} are selected in the ratio 1: 2.2: 3.7. Accordingly, $L_{m1} = 100nH$, $L_{m2} = 220nH$, and $L_{m3} = 370nH$ are chosen. To further clarify the proposed concept, the di/dt at different fault locations (F_1–F_6) is analyzed based on the grid specifications provided in Table I, and the resulting voltages across the measurement inductors are calculated and summarized in Table II.

The detection threshold must be selected such that, if a fault occurs at the beginning of the last section (F_5), CB_2 does not react, while a fault occurring at the end of the section closest to the source (F_2) reliably triggers CB_1. Accordingly, based on the results in Table II, the threshold should be selected within the range 1.571- 1.666, enabling coordinated operation of the circuit breakers using a single unified threshold for the considered sample network.

B. Fault Evolution in a Radial DC Microgrid With Multiple Resistive Loads

This case corresponds to a scenario that has been extensively investigated in prior studies. In this configuration, all buses are connected to purely resistive loads ($P_1, P_2, P_3 \neq 0$). The distinguishing factor between this case and the preceding one is the specific loop in which the fault occurs.

As an illustrative example, when a fault takes place at location F_6, the immediate fault loop is formed by load P_2, breaker 3, and transmission line 3. Load P_2 is located between transmission lines 2 and 3, both of which are modeled as inductive elements. Due to the inductive nature of these transmission lines, their currents cannot change instantaneously at the moment of fault inception. Consequently, the current through load P_2 also remains unchanged immediately after the fault. Furthermore, since load P_2 is assumed to be purely resistive, the voltage at the corresponding bus remains constant in the immediate post-fault interval.

Under these assumptions, the initial di/dt experienced by CB_3 immediately following fault inception can be expressed as follows:

$$F_6 \rightarrow (di/dt)_{@CB_3}(t = t_0^+) = \frac{V_3(t=t_0^-) - R_{34} i_{34}(t=t_0^-)}{l_{fcl} + l_{34}} \quad (5)$$

Neglecting the voltage drop across line resistances, the initial rate of increase of the fault current through CB_3 can be derived analogously to the previous case by considering the di/dt of the transmission lines and the fault current limiter.

$$F_6 \rightarrow (di/dt)_{@CB_3} \approx \left(\frac{1}{(di/dt)_{fcl}} + \frac{1}{(di/dt)_{l34}}\right)^{-1} \quad (6)$$

$$F_5 \rightarrow (di/dt)_{@CB_3} = (di/dt)_{fcl} \quad (7)$$

The analytical expressions derived in (5) and (6) can be generalized to describe the immediate fault loop when a fault occurs at any location within the grid. Notably, only in the immediate fault loop does the maximum current rise rate, occur at the instant of fault inception. For circuit breakers located in other loops, a sudden increase in di/dt is not expected at the fault instant. Instead, the maximum rise rate is expected to occur after a certain delay. This delay depends directly on the network parameters, particularly the connected loads as well as the line and fault inductances. In this study, the protection thresholds are selected such that only one circuit breaker reaches its threshold for a given fault. Nevertheless, the temporal separation between the instants of maximum current rise rates experienced by different breakers can be exploited to design an effective backup protection strategy.

For circuit breakers located in the loop in close vicinity to the source (CB_1), the post-fault source voltage can be assumed to remain approximately constant. Under this assumption, the maximum di/dt, can be calculated explicitly using the methodology presented in the previous scenario. If the fault occurs within the same loop, this maximum di/dt is attained immediately after fault inception. Conversely, if the fault is located in a different loop, the maximum current rise rate occurs at a later time, depending on the grid parameters; however, the magnitude of the maximum di/dt remains unchanged.

For all remaining circuit breakers that are neither part of the immediate fault loop nor located in close vicinity to the source, the evolution of the di/dt is governed by the time constants associated with the voltage decay at the buses connected to the line in which the breaker is installed. Specifically, di/dt depends on the rates at which the voltages at the two terminal buses decrease following a fault.

TABLE III. COORDINATION STRATEGY PERFORMANCE EVALUATION (MULTI-RESITIVE LOAD SCENARIO)

	Max. voltage across L_{mi} (V)			**Does CB react?**		
Location	$V(L_{m1})$	$V(L_{m2})$	$V(L_{m3})$	CB_1	CB_2	CB_3
F_1	10	< 0	< 0	✓	✗	✗
F_2	1.666	< 0	< 0	✓	✗	✗
F_3	1.428	12	< 0	✗	✓	✗
F_4	0.769	1.713	< 0	✗	✓	✗
F_5	0.714	1.498	15	✗	✗	✓
F_6	0.465	0.774	1.764	✗	✗	✓

As an illustrative example, if a fault occurs at location F_5, the di/dt experienced by CB_2 is determined by the voltage decay dynamics of Buses 2 and 3. The voltage drop time constant of each bus can be calculated based on the load resistance connected to that bus and the inductance between the bus and the fault location. Denoting the voltage decay time constants of Buses 2 and 3 as τ_2 and τ_3, respectively, the resulting di/dt at CB_2 depends on the relative rate at which the voltage at Bus 3 decreases compared to that at Bus 2.

When τ_2 and τ_3 are equal, the maximum current rise rate, di/dt, can be calculated using the same methodology presented for the previous scenario. However, τ_2 and τ_3 are functions of the connected loads and the fault inductance. Since a fault may occur at any location along Line 34 and the load conditions may vary, the protection thresholds must be selected such that selectivity is preserved under all fault contingencies. Consequently, the maximum possible di/dt experienced by CB_2 must be determined in order to appropriately define its threshold. The maximum di/dt at CB2 occurs when τ_3 is minimized, corresponding to the fastest voltage decay at Bus 3. Therefore, to determine the worst-case di/dt, the fault inductance must be minimized and the load resistance connected to Bus 3 must be maximized. This condition corresponds to a fault occurring at the beginning of Line 34 (F_5) combined with an infinite load resistance (i.e., no load), which results in the maximum di/dt for CB_2.

$$F_5 \rightarrow Max\ (di/dt)_{@CB_2} = \frac{V_2(t=t_0^-) - R_{23} i_{23}(t=t_0^-)}{2l_{fcl} + l_{23}} \quad (8)$$

$$F_5 \rightarrow Max(di/dt)_{@CB_2} \approx \left(\frac{2}{(di/dt)_{fcl}} + \frac{1}{(di/dt)_{l23}}\right)^{-1} \quad (9)$$

In this scenario, to establish a unified protection threshold across the network, the measurement inductances are selected to be proportional to the lengths of the lines for which the maximum current rise rates have been calculated. Accordingly, unlike the previous scenario, the measurement inductances L_{m1}, L_{m2}, and L_{m3} are selected in the ratio 1: 1.2: 1.5. Accordingly, $L_{m1} = 100nH$, $L_{m2} = 120nH$, and $L_{m3} = 150nH$ are chosen. The corresponding results are calculated and summarized in Table III. As evident from these results, any threshold value within the range of 1.498- 1.666 ensures selective protection.

C. Fault Evolution With Multiple R-C Loads

The inclusion of capacitors increases the complexity of the analytical framework. However, this does not necessarily imply an increase in the fault current rise rate. On the contrary, under typical operating conditions, capacitors tend to

result in a smoother fault transient. As discussed in the previous section, the rate of rise of the fault current experienced by each circuit breaker is governed by the manner in which the bus voltages decay in response to a fault.

In the presence of very small capacitances with low equivalent series resistance (ESR), the capacitor voltage decay may exhibit oscillatory behavior, which can lead to high values of inductor di/dt. By applying the superposition principle, the contribution of each capacitor and source can be analyzed independently. At the instant of fault inception, each capacitor forms a series RLC circuit, whose transient response is determined by the relationship between $\alpha = R/2L$ and the natural frequency $\omega_0 = 1/\sqrt{LC}$. In practical DC microgrids, DC-link capacitors are typically large in order to support the load for a specified duration, and larger capacitance values are generally associated with higher ESR. In combination with relatively short line lengths, this configuration is likely to result in an overdamped voltage response. Under overdamped conditions, the bus voltages do not undershoot their steady-state values, and consequently, the resulting di/dt remains within the bounds described in the previous scenario. The rate of rise of the fault current in the immediate fault loop remains unchanged, while circuit breakers in other loops may experience even lower di/dt due to the smoother voltage decay. Therefore, under overdamped conditions, the coordination strategy developed in the previous scenario remains valid.

Nevertheless, long line lengths or small capacitance values may give rise to an underdamped response. To ensure that the system operates within the overdamped regime, a load-flow-based analysis of the network parameters is required.

III. Simulation Verification

This section presents the simulation results obtained for the sample grid shown in Fig. 2, using the system specifications summarized in Table I. All three predefined scenarios are implemented in MATLAB/Simulink to evaluate the proposed threshold selection strategies. In all cases, a solid fault is applied at $t = 0.01s$ at various locations (F_1–F_6), and the measured voltages are evaluated against the preselected protection thresholds.

A. Single Loop Fault Simulation Results

Fig. 3 presents the MATLAB/Simulink simulation results for the voltages measured across the sensing inductors during fault events under Scenario A. In this scenario, P_1 and P_2 are set to zero, while $P_3 = 16kW$. A solid fault with a resistance of 1 mΩ is applied at various locations (F_1–F_6), and the resulting voltages across the measurement inductances ($L_{m1} = 100nH$, $L_{m2} = 220nH$, and $L_{m3} = 370nH$) are evaluated against a unified threshold of 1.63 V, indicated by the red dashed line. As shown, for each fault condition, only the upstream circuit breaker closest to the fault reaches the threshold, while the others remain below it. This behavior confirms the effectiveness of the proposed unified threshold coordination strategy.

B. Fault Evolution in a Radial DC Microgrid With Multiple Resistive Loads

Fig. 4 presents analogous simulation results for the voltages measured across the sensing inductors under Scenario B. In this scenario, P_1, P_2, and P_3 are set to 32 kW, 32 kW, and

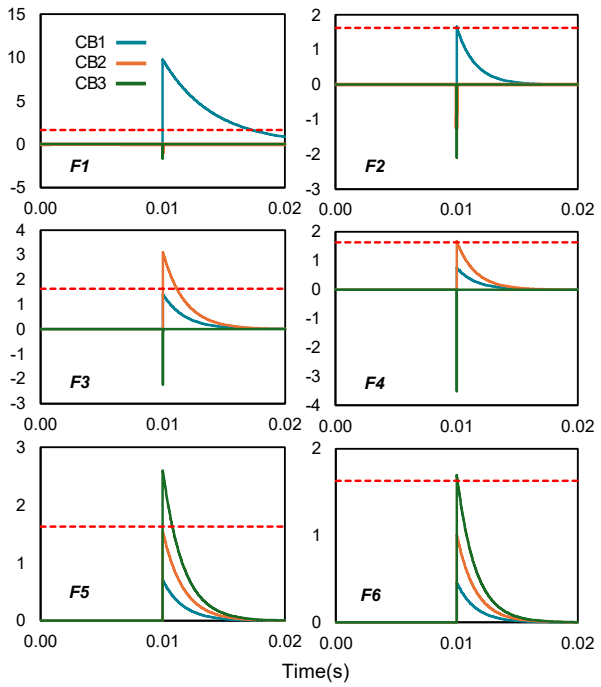

Fig. 3. L_{mi} voltages for Scenario "A" at different locations (F_1–F_6).

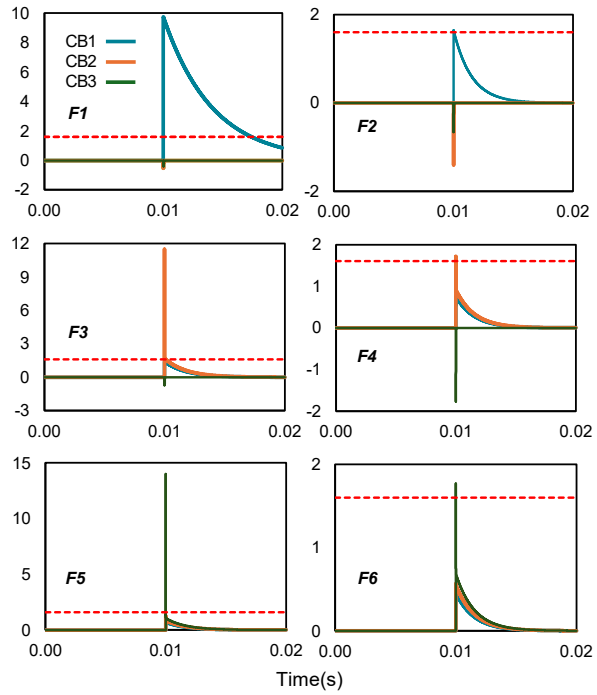

Fig. 4. L_{mi} voltages for Scenario "B" at different locations (F_1–F_6).

16 kW, respectively. A fault with a resistance of 1 mΩ is applied at various locations (F_1–F_6), and the resulting voltages across the measurement inductances ($L_{m1} = 100nH$, $L_{m2} = 120nH$, and $L_{m3} = 150nH$) are evaluated against a unified threshold of 1.6 V. Similar to the previous scenario, only the upstream circuit breaker closest to the fault reaches the threshold, while the remaining breakers stay below it.

C. Fault Evolution in a Radial DC Microgrid With Multiple R-C Loads

Fig. 5 presents similar simulation results for the voltages measured across the sensing inductors under Scenario C. In

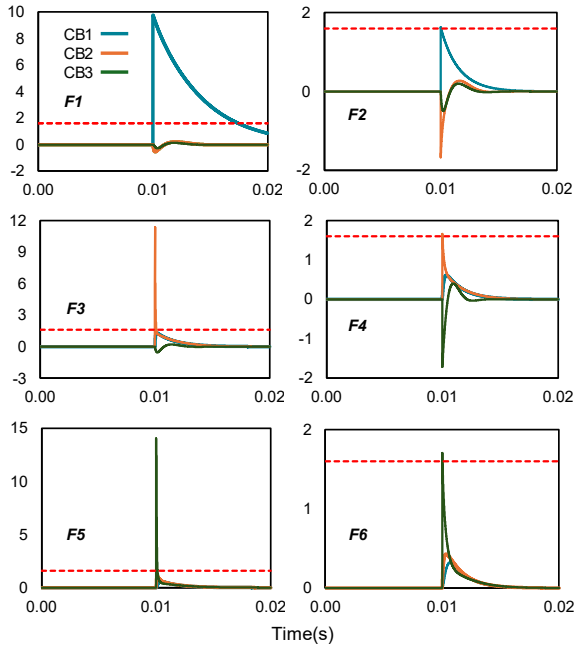

Fig. 5. L_{mi} voltages for Scenario "C" at different locations (F_1–F_6).

this scenario, P_1, P_2, and P_3 are set to 32 kW, 32 kW, and 16 kW, respectively. In contrast to the previous scenarios, capacitive elements are included. A 10 mF capacitor with an ESR of 0.1 Ω is connected in parallel with each 32 kW load, while a 5 mF capacitor with an ESR of 80 mΩ is connected in parallel with the 16 kW load.

A fault with a resistance of 1 mΩ is applied at various locations (F_1–F_6), and the resulting voltages across the measurement inductances ($L_{m1} = 100nH$, $L_{m2} = 120nH$, and $L_{m3} = 150nH$) are evaluated against a unified threshold of 1.6 V. Similar to the previous scenarios, only the upstream circuit breaker closest to the fault reaches the threshold, while the remaining breakers remain below it.

IV. Conclusion

This paper proposed a protection coordination strategy for radial DC microgrids based on the rate of rise of fault current rather than the conventional fault current magnitude, directly addressing the challenges posed by extremely fast fault transients in low-inductance DC networks. An analytical framework was developed to systematically derive di/dt thresholds for circuit breakers at different locations, enabling selective and fast fault isolation. While this work established a coordination methodology based on a unified threshold setting combined with graded measurement inductances, the proposed framework is not restricted to a single global threshold. In practical systems with variable load conditions and fixed hardware parameters, the use of breaker-specific di/dt thresholds provides an additional degree of freedom that can be exploited to further enhance coordination robustness and reliability.

Acknowledgment

This work was supported in part by the Helmholtz Association under the program "Energy System Design" and under the Helmholtz Young Investigator Group "Hybrid Networks" under Grant VH-NG-1613, and in part by the Indo-German Science and Technology Centre (IGSTC), through Paired Early Career Fellowship in Applied Research (PECFAR) Award 2025, under Grant IGSTC/PECFAR-2025/05937/MG-DK/43/2025-26/156. The work of Satish Naik Banavath was supported by the Anusandhan National Research Foundation (ANRF), Department of Science and Technology (DST), India, under Grant EEQ/2023/000017.

References

[1] S. N. Banavath, A. Pogulaguntla, G. De Carne, M. Joševski and R. Singh, "Transformative Role of Solid-State Circuit Breakers in Advancing DC Systems for a Sustainable World," in IEEE Power Electronics Magazine, vol. 11, no. 4, pp. 61-72, Dec. 2024.

[2] R. Rodrigues, Y. Du, A. Antoniazzi and P. Cairoli, "A Review of Solid-State Circuit Breakers," in IEEE Transactions on Power Electronics, vol. 36, no. 1, pp. 364-377, Jan. 2021.

[3] A. R. F. Bento, F. Bento and A. J. M. Cardoso, "A Review on Hybrid Circuit Breakers for DC Applications," in IEEE Open Journal of the Industrial Electronics Society, vol. 4, pp. 432-450, 2023.

[4] G. Chavan, X. Song, D. Chatterjee, A. Patni and P. Cairoli, "Coordination of Solid-State Circuit Breakers for DC Grids Under High-Fault-di/dt Conditions," 2022 IEEE Energy Conversion Congress and Exposition (ECCE), Detroit, MI, USA, 2022.

[5] R. Kheirollahi, S. Zhao, H. Zhang, X. Lu, J. Wang and F. Lu, "Coordination of Ultrafast Solid-State Circuit Breakers in Radial DC Microgrids," in IEEE Journal of Emerging and Selected Topics in Power Electronics, vol. 10, no. 4, pp. 4690-4702, Aug. 2022.

[6] A. Meghwani, S. C. Srivastava and S. Chakrabarti, "A Non-unit Protection Scheme for DC Microgrid Based on Local Measurements," in IEEE Transactions on Power Delivery, vol. 32, no. 1, pp. 172-181, Feb. 2017.

[7] Y. Bai and A. Rajapakse, "Fault Detection and Localization in a Ring Bus DC Microgrid Using Current Derivatives," 2020 IEEE Canadian Conference on Electrical and Computer Engineering (CCECE), London, ON, Canada, 2020.